Three-Dimensional Self-Standing and Conductive $MnCO_3$@Graphene/CNT Networks for Flexible Asymmetric Supercapacitors

Shuxing Wu,[†] Canbin Liu,[†] Kwan San Hui,[*,‡] Kwun Nam Hui,[*,§] Je Moon Yun,[∥] and Kwang Ho Kim[*,∥,⊥]

[†]School of Chemical Engineering and Light Industry, Guangdong University of Technology, Guangzhou 510006, PR China

[‡]School of Mathematics, University of East Anglia, Norwich, NR4 7TJ, United Kingdom

[§]Institute of Applied Physics and Materials Engineering, University of Macau, Avenida da Universidade, Taipa, Macau, China

[∥]Global Frontier R&D Center for Hybrid Interface Materials, Pusan National University, 30 Jangjeon-dong, Geumjung-gu, Busan 609-735, South Korea

[⊥]School of Materials Science and Engineering, Pusan National University, San 30 Jangjeon-dong, Geumjeong-gu, Busan 609-735, Republic of Korea

[*]*Corresponding author:*

E-mail: bizhui@umac.mo (K.N. Hui)

Tel: +853 8822-4426; Fax: +853 8822-2426

E-mail: kwhokim@pusan.ac.kr (Kwang Ho Kim)

Tel.: +82 51 510 3391; Fax: +82 5 1514 4

ABSTRACT

The practical applications of flexible supercapacitor depend strongly on the successful fabrication of advanced electrode materials with high electrochemical performance. Herein, three-dimensional conductive network-based self-standing $MnCO_3$@graphene/CNT hybrid film fabricated by combining hydrothermal treatment and vacuum filtration for flexible solid-state supercapacitors is reported. Ingenious $MnCO_3$@graphene structure is embedded in a porous CNT network, in which monodispersed $MnCO_3$ nanorod is well confined in graphene nanosheets. This hierarchical structure provides rapid electron/electrolyte ion transport pathways and exhibits excellent structural stability, resulting in rapid kinetics and long lifecycle. The $MnCO_3$@graphene/CNT electrode delivers a high specific capacity of 467.2 F g^{-1} at 1 A g^{-1} with 84.3% capacitance retention when the current density is increased from 1 to 10 A g^{-1}. An asymmetric supercapacitor (ASC) is fabricated with the $MnCO_3$@graphene/CNT film as positive electrode and carbon cloth/activated carbon as negative electrode. The ASC device exhibits a high energy density of 27 W h kg^{-1} at a power density of 1622.7 W kg^{-1}. Remarkably, the device exhibits 93% capacitance retention after 6000 cycles.

KEYWORDS: $MnCO_3$, CNT, Graphene, Flexible Asymmetric Supercapacitor

INTRODUCTION

In recent years, flexible supercapacitor has attracted considerable attention in wearable and lightweight electronic devices, such as smartphones, e-readers, and bendable electronic gadgets owing to its fast charging–discharging capacity, high power density, long lifespans, and remarkable flexibility.[1, 2] Besides, flexible supercapacitors offer distinctive advantage of the stability and safety because of the use of gel-like solid-state electrolyte, which eliminates the safety issue aroused from the leakage of electrolyte and short circuit issues.[3] However, flexible supercapacitors suffer from the low energy density that hinders their practical application. Development of electroactive materials possessing high specific capacitance, superior conductivity, good mechanical properties, and high stability is one of the keys for fabricating flexible all-solid-state supercapacitor.[4]

Electrochemical active $MnCO_3$ is regard as a potential cathode material for supercapacitors owing to its redox-richness and low-manganese valence (+2).[5, 6] Meanwhile, $MnCO_3$ is earth abundant, environmentally friendly, and often utilized as sacrificial template for Mn-based materials synthesis. When applied as a supercapacitor electrode, stable rhodochrosite structure of $MnCO_3$ could stabilizes the [MnO_6] octahedral structure via [CO_3] planes during charge–discharge cycles.[5] Zhang et al.[7] prepared $MnCO_3$ nanospheres by precipitation method and exhibited a specific capacity of 129 F g^{-1} at 0.15 A g^{-1}. Tang et al.[5] reported peanut-like $MnCO_3$ microcrystals, which exhibited a specific capacitance of 293.7 F g^{-1} and 71.5% retained specific capacitance after 6000 cycles. Nevertheless, critical drawbacks including low specific capacitance, limited conductivity, and poor cycling performance, hinder the application of $MnCO_3$ as electrode material for supercapacitors.[8] Building nanohybrids with carbonaceous materials that serve as structural buffer and electroactive material is an effective approach to overcome the abovementioned drawbacks.[9, 10] In particular, graphene is well-regarded a promising carbon matrix because of its remarkable physical properties, such as high

conductivity[11], superb mechanical flexibility[12], and large surface area[13]. Thus, many reports regarding the enhancement of electrochemical performance of $MnCO_3$/graphene composites have been reported.[14-18] However, the reported $MnCO_3$/graphene composites still suffer from the unsatisfactory rate capability and short cycling performance due to the non-intimate contact between $MnCO_3$ and graphene.

Herein, the encapsulation of $MnCO_3$ nanorod within graphene nanosheet ($MnCO_3$@graphene) is realized via a cost-effective, one-pot hydrothermal method. Each $MnCO_3$ nanorod is well wrapped by graphene rather than being deposited on the surface of graphene or aggregated within the graphene sheets. Finally, a lightweight, thin, and self-standing $MnCO_3$@graphene/CNT film is fabricated by the vacuum filtration of mixed $MnCO_3$@graphene and CNT dispersion. The $MnCO_3$@graphene/CNT electrodes exhibit a specific capacitance of 467.2 F g^{-1} at 1 A g^{-1}, which is approximately 1.5 times higher than $MnCO_3$@graphene electrodes (322.1 F g^{-1} at 1 A g^{-1}). A flexible asymmetric all-solid-state supercapacitor (ASC) with a high output cell voltage of 1.8 V is fabricated using such $MnCO_3$@graphene/CNT as a positive electrode, carbon cloth/activated carbon (CC/AC) as a negative electrode, and Na_2SO_4/poly(vinyl alcohol) (PVA) as a solid electrolyte. The ASC delivers an energy density of 27 W h kg^{-1} at a high-power density of 1622.7 W kg^{-1} and excellent cyclability (capacity retention of 93% for 6000 cycles).

EXPERIMENTAL SECTION

Preparation of Graphite Oxide. Flake graphite (Asbury Carbons) was used to synthesize graphite oxide following the modified Hummers' method.[19, 20] First, graphite flakes (3 g) was added into the concentrated sulfuric acid (H_2SO_4, 70 mL) at room temperature (RT), and sodium nitrate ($NaNO_3$, 1.5 g) was added to the solution. Subsequently, potassium permanganate ($KMnO_4$, 9.0 g) was added slowly to maintain the suspension temperature at

15 °C under vigorous stirring in an ice bath. Successively, the mixture was stirred at 35 °C for 30 min and diluted with deionized (DI) water (140 mL). Then, DI water (500 mL) and hydrogen peroxide solution (H_2O_2, 30 wt%, 20 mL) were added successively. Finally, the mixture was filtered and washed with 1:10 HCl aqueous solution (250 mL), followed by washing with DI water and centrifugation. The solution was freeze-dried to obtain brownish powder.

Preparation of $MnCO_3$@Graphene. The present amount of $KMnO_4$ with $KMnO_4$/graphene oxide (GO, 1 mg mL^{-1}) weight ratio of 10:3 was added into the GO solution, and the mixture (30 mL) was then transferred into a 50 mL Teflon-lined stainless-steel autoclave and held at 180 °C for 12 h before cooling down to RT naturally.[17] After hydrothermal treatment, the as-obtained sample was washed with DI water for several times. The elemental composition of the $MnCO_3$@Graphene was determined by inductively coupled plasma mass spectrometry (Thermo Fisher, ICAP RQ). And the mass ratio of $MnCO_3$ in the composite was calculated to be 80.0%.

Preparation of $MnCO_3$@Graphene/CNT. The self-standing $MnCO_3$@graphene/CNT film was obtained simply by using vacuum filtration method. Single-walled CNT (50 mg, Iljin Nanotech) was added in DI water (100 mL), and then probe sonicated to ensure the sufficient mix. After that, the CNT dispersion (15 mL) was mixed with the well-dispersed $MnCO_3$@graphene (72 mg) in 30 mL DI water under vigorous stirring for 60 min. The as-obtained solution was obtained by vacuum filtration by a polytetrafluoroethylene membrane (0.2 μm pore size, 47 mm in diameter; SciLab), and a self-standing film was carefully removed off from the membrane. The areal density of the hybrid film is 4.04 mg cm^{-2}.

Characterization. The morphology and structure of the samples were investigated by scanning electron microscope (SEM; Hitachi, S-4800), transmission electron microscopy (TEM; FEI Talos, USA), X-ray powder diffraction (XRD; Rigaku MPA-2000 with Cu kα radiation in the

2θ range from 5° to 80°), X-ray photoelectron spectroscopy (XPS; AXIS SUPRA), and Raman spectrometer (XperRam 200).

Electrochemical Measurements. Electrochemical performances were tested with electrochemical station (IVIUM Nstat) in three-electrode test for single electrodes and in a two-electrode system for flexible ASC devices. In the three-electrode test, platinum foil, saturated calomel electrode (SCE, Hg/Hg_2Cl_2), and 1 M $NaSO_4$ solution were used as the counter electrode, reference electrode, and the electrolyte, respectively.[21, 22] Paper-type samples (1 cm × 1 cm) were used as the working electrode. The specific capacitance (C_s, F g^{-1}) of a single electrode was calculated from galvanostatic charge-discharge (GCD) curves according to the equation,

$$C_s = \frac{I \times \Delta t}{m \times \Delta V}, \quad (1)$$

where I (A), Δt (s), m (g), and ΔV (V) represent the applied specific discharge current, the time for a full discharge, the mass of the active material, and the voltage window for one scanning segment, respectively.

The flexible ASC was fabricated with $MnCO_3$@graphene/CNT as the positive electrode, CC/AC as the negative electrode, and Na_2SO_4/PVA as the solid electrolyte. The CC/AC electrode was fabricated similarly as the aforementioned preparation of individual electrode, except that the current collector was CC (2 cm × 2 cm) (AvCarb 1071 HCB). The CC was sonicated in acetone, ethanol, and DI water for 30 min before use. The Na_2SO_4/PVA was prepared as follows: Na_2SO_4 (6 g) and PVA (6 g) were dissolved in DI water (60 mL) with vigorous and continuous stirring at 90 °C for 1 h.[23] Gold-coated polyethylene terephthalate (PET) membrane was used as the conductive substrate. Prior to assembling, $MnCO_3$@graphene/CNT and CC/AC electrode were soaked into the Na_2SO_4/PVA gel electrode for 2 h, and then maintained at 80 °C for 12 h to remove excess water. Finally, they were

assembled together under pressing.

To obtain charge balance, the AC (m_-) to $MnCO_3$@graphene/CNT (m_+) mass ratio (2.75) was obtained according to the equation,

$$\frac{m_+}{m_-} = \frac{C_-\Delta V_-}{C_+\Delta V_+}, \quad (2)$$

For the assembled flexible ASC, specific capacitances (C_{asy}, F g^{-1}), energy density (E, Wh kg^{-1}), and power density (P, W kg^{-1}) were calculated as follows:

$$C_{asy} = \frac{I \times \Delta t}{M \times \Delta V}, \quad (3)$$

$$E = \frac{1}{2}\frac{1000 C_{asy} \Delta V^2}{3600}, \quad (4)$$

$$P = \frac{3600E}{\Delta t}. \quad (5)$$

RESULTS AND DISCUSSION

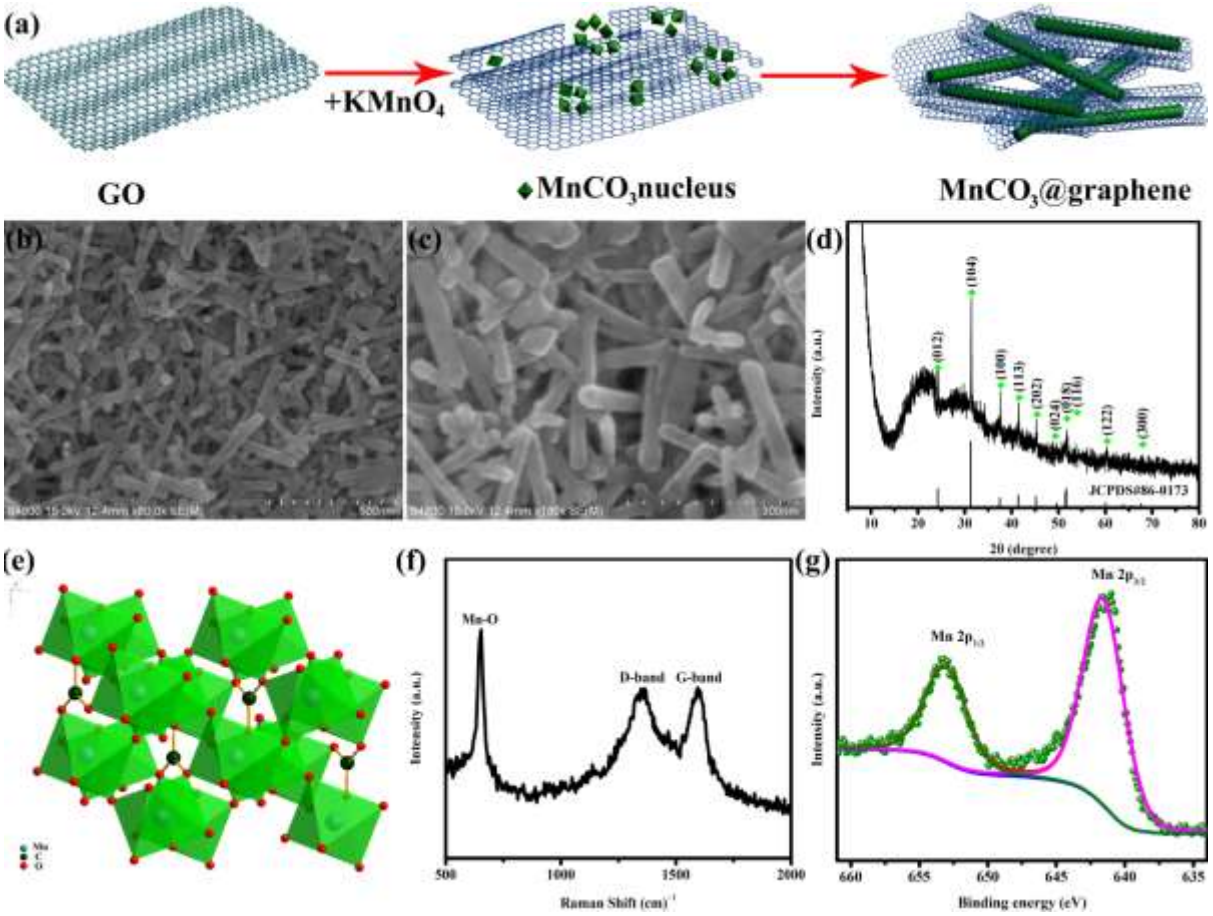

Figure 1. (a) Proposed $MnCO_3$@graphene evolution process. (b and c) SEM images and (d) XRD pattern of $MnCO_3$@graphene, (e) crystal structure of $MnCO_3$. (f) Raman spectrum of $MnCO_3$@graphene. (g) XPS spectrum of Mn 2p.

Figure 1a shows the preparation of the $MnCO_3$@graphene composites. The formation of Mn^{2+} is easier than that of MnO_2 in the current hydrothermal process by comparing the electrode potential according to the Nernst equation.[17] And the rod-like shape is generated through the rolling mechanism.[24] A possible mechanism is proposed as follows: Permanganate is reduced into Mn^{2+} ions and further electrostatically bond with the O atoms of the negatively charged oxygen functional groups on graphene sheets as anchor sites. At the same time, graphene was reduced from graphene oxide. Under the hydrothermal conditions, $MnCO_3$ nuclei appear first in the solution, and then $MnCO_3$ nanosheets formed through a condensation reaction.

Subsequently, the sheet-like structure of $MnCO_3$ curls into nano-rod. $MnCO_3$ was formed along the graphene nanosheet framework during the hydrothermal process, leading to the wrapping of graphene nanosheets on the surface of $MnCO_3$ nanorods. SEM images of as-synthesized $MnCO_3$@graphene reveals all particles are rod-like and monodispersed with a length approximately <300 nm and nominal diameter of 15–30 nm (Figure 1b and c). Almost no graphene nanosheets are observed in the SEM images, suggesting $MnCO_3$ nanorods are well wrapped by few-layer graphene. Additionally, small amount of graphene sheets can be found in the low-magnification SEM images and the graphene wrapped $MnCO_3$ nanorods are in mutual contact to form film-like structure (Figure S1). Structural features of $MnCO_3$@graphene are characterized using XRD, Raman spectroscopy, and XPS. Figure 1d shows the XRD pattern of $MnCO_3$@graphene. The XRD pattern displays a broad diffraction peak at 22.6°, referring to the characteristics of graphene and verifying its existence in $MnCO_3$@graphene,[25] while other peaks are matched well to the rhodochrosite phase of $MnCO_3$ (JCPDS card No. 86-0173). Figure 1e shows the crystal structure of $MnCO_3$ where MnO_6 octahedra and CO_3 equilateral triangles are in the same plane perpendicular to the *z*-axis [26]. A notable Mn-O vibrational band appears at 653.1 cm^{-1}, demonstrating the presence of $MnCO_3$ in $MnCO_3$@graphene (Figure 1f).[8] The two peaks at ca. 1364 and ca. 1594 cm^{-1} correspond to sp^3-type disordered carbon (D-band) and sp^2-type ordered graphitic carbon (G-band), respectively.[27] The I_D/I_G value of $MnCO_3$@graphene (1.0) is higher than that of the GO (0.93) (Figure S2), which is indicative of the reduction of GO with more defects and disordered structure.[28] A complete survey of $MnCO_3$@graphene in Figure S3 shows the presence of Mn 2p, Mn 2s, Mn 3s, Mn3p, O1s, and C1s, with no evidence of impurities. The high-resolution Mn 2p spectrum in Figure 1g shows two obvious peaks at binding energy of 641.6 and 653.1 eV, corresponding to Mn $2p_{3/2}$ and Mn$2p_{1/2}$ of Mn^{2+} in $MnCO_3$, respectively.[5, 29]

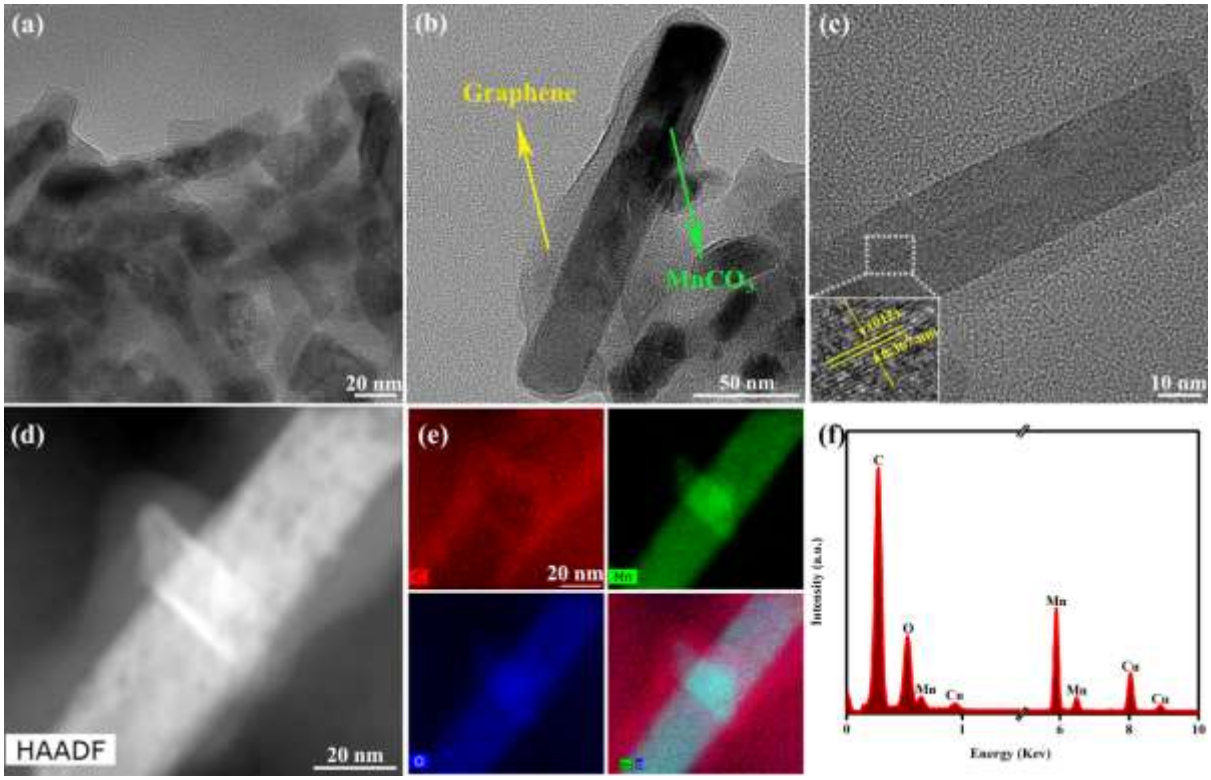

Figure 2. (a, b, and c) TEM images of $MnCO_3$@graphene at different magnifications. The inset of (c) shows an HRTEM image of the $MnCO_3$@graphene. (d and e) HAADF-STEM image and corresponding elemental mapping images of $MnCO_3$@graphene. (f) EDX result of $MnCO_3$@graphene. Cu signals are from copper grid.

TEM and high-resolution TEM (HRTEM) analyses are performed to understand the architecture of $MnCO_3$@graphene active materials better. Figure 2a presents that all the $MnCO_3$ nanorods are thoroughly wrapped by flexible and ultrathin graphene sheets. The graphene nanosheets not only encapsulate the $MnCO_3$ nanorods but also interconnect neighboring nanorods. The bridging graphene sheets with high conductivity are envisioned to provide high efficient electronic connections for the monodispersed $MnCO_3$ nanorods.[30] Meanwhile, the specific structure was expected to reinforce the mechanical stability of the electrode material and prevent the $MnCO_3$ nanorods from aggregating and the electrochemical

dissolution during cycling.[31] Figure 2b shows obvious interface between the $MnCO_3$ nanorod and the attached graphene sheet. Figure 2c shows the HRTEM image of one $MnCO_3$@graphene nanorod, in which the measured interplanar spacings of 0.367 nm for the well-resolved lattice fringes consist well with the rhodochrosite $MnCO_3$ (012) planes. Further high-angle annular dark-field scanning transition electron microscopy (HAADF-STEM) image and element mapping analysis (Figure 2d, e) demonstrate that the Mn, O, and C elements are uniformly distributed along the $MnCO_3$@graphe. A typical energy-dispersed X-ray spectroscopy (EDS) spectrum (Figure 2f) shows characteristic peaks of the elements, proving the coexistence of Mn, C, and O, and no impurities can be detected.

Figure 3 illustrates the fabrication process of the flexible and self-standing $MnCO_3$@graphene/CNT film. Figure 3e shows the digital images of the $MnCO_3$@graphene/CNT film (37 mm in diameter). In addition, the film could be easily wrapped around a glass rod without any obvious mechanical damage, demonstrating its flexibility and durability. Figure 3f and S4 show the cross-section SEM image of the $MnCO_3$@graphene/CNT film, revealing the uniform hybrid film with an average thickness of 10 μm. The $MnCO_3$@graphene composites were trapped in the porous CNT network, which offers several major advantages for high performance supercapacitors. (1) The intimate contact between the $MnCO_3$@graphene and CNTs provides high electrical conductivity; (2) the interpenetrating $MnCO_3$@graphene/CNT film possesses open channels, ensuring effective electrolyte transport and active-site accessibility; (3) the CNT, serving as electrode and current collector, produces film with high flexibility and high mechanical strength.[32, 33] Notably, the synergistic effects of $MnCO_3$@graphene and CNT could lead to a high flexibility electrochemical performance for $MnCO_3$@graphene/CNT films.

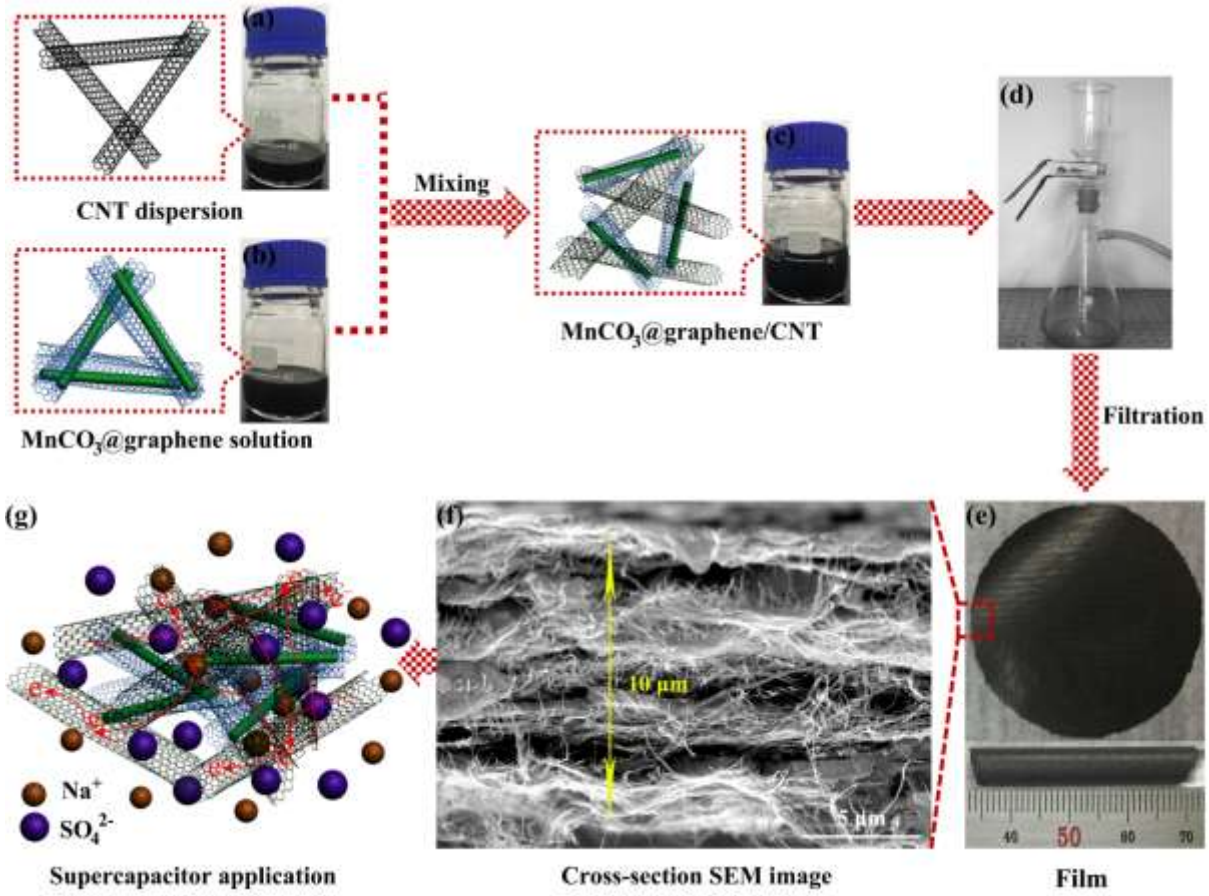

Figure 3. Schematics of the fabrication process of $MnCO_3$@graphene/CNT papers: (a) CNT and stable CNT dispersion. (b) $MnCO_3$@graphene and stable $MnCO_3$@graphene dispersion. (c) CNT and $MnCO_3$@graphene hybrid and the stable hybrid dispersion. (d) Vacuum filtrati on was used in the fabrication process. (e) Digital photographs of the flexible and self-standing $MnCO_3$@graphene/CNT papers and wrapping of glass rod. (f) Cross-section SEM image of the $MnCO_3$@graphene/CNT papers with a thickness of 10 μm. (g) Sup ercapacitor applications of the $MnCO_3$@graphene/CNT papers and schematic of the mechani sm involved in the rapid electron transport and ion diffusion of the unique structure.

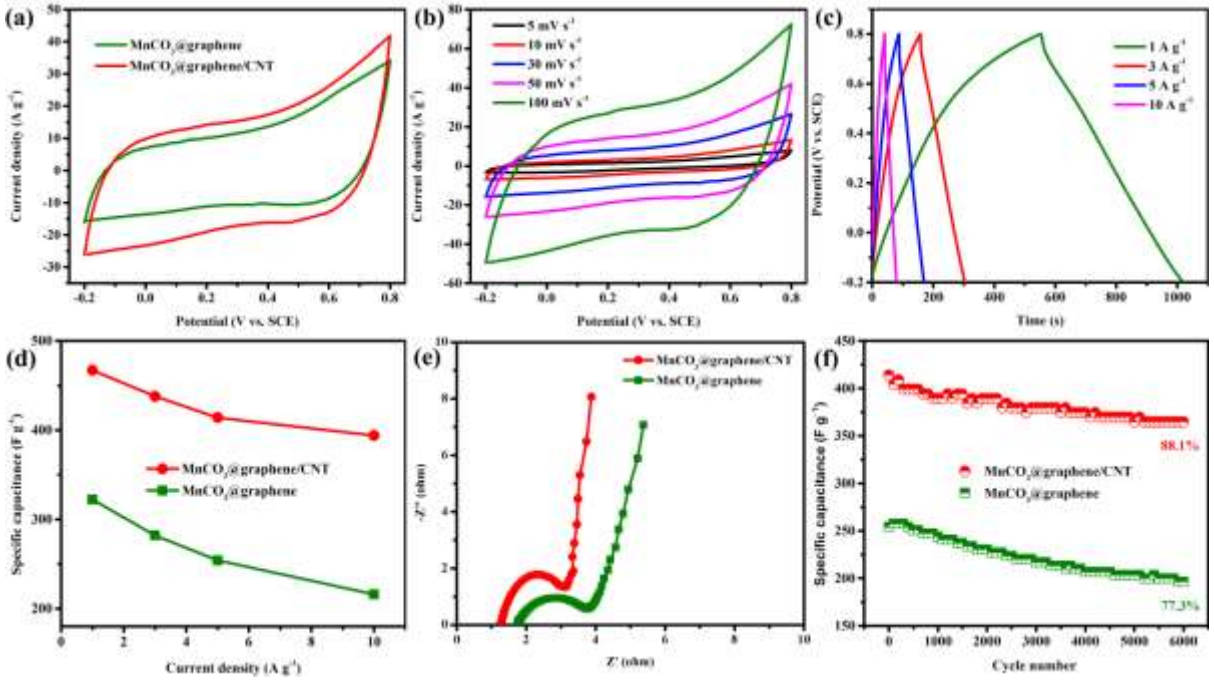

Figure 4. (a) Comparison of CV curves of two different electrodes at 50 mV s^{-1}. (b) CV curves of $MnCO_3$@graphene/CNT electrode at different scan rates. (c) GCD curves of $MnCO_3$@graphene/CNT electrode at different current densities. (d) Specific capacitances of the two electrodes at different current densities. (e) Nyquist plots of the electrodes. (f) Cycle performance of the two electrodes at 5 A g^{-1} for 6000 cycles.

To evaluate the electrochemical performance of the $MnCO_3$@graphene and $MnCO_3$@graphene/CNT, samples were tested as working electrode in 1 M Na_2SO_4 aqueous electrolyte solution using a three-electrode configuration with a SCE reference electrode. Figure 4a shows the CV curves of $MnCO_3$@graphene and $MnCO_3$@graphene/CNT at a scan rate of 50 mV s^{-1}. Both CV curves are nearly ideal symmetrical rectangular shape in wide potential window of −0.2 V to 0.8 V, revealing excellent capacitive behavior.[34, 35] The reversibly redox reactions occurred on $MnCO_3$ in $NaSO_4$ solution can be considered as follows:[14]

$$MnCO_3 + Na^+ + e^- \leftrightarrow NaMnCO_3 \quad (6)$$

The redox processes result in pseudocapacitance of $MnCO_3$. Notably, the enlarged CV curve areas of $MnCO_3$@graphene/CNT suggest higher specific capacitance than $MnCO_3$@graphene, which could be attributable to the synergistic effects of $MnCO_3$@graphene and CNT. Figure 4b shows the CV curves for the $MnCO_3$@graphene/CNT electrode with increasing scan rate from 5–100 mV s^{-1}. The shape of the curves is well-retained up to 100 mV s^{-1}, indicating a fast charge transportation characteristic of the electrolyte, interfaces, and electrode structure of the $MnCO_3$@graphene/CNT.[36-38] Figure 4c shows the GCD curves of $MnCO_3$@graphene/CNT at various current densities. All the curves show good symmetry and nearly linear slopes, indicating the capacitive characteristic and good reversibility of the $MnCO_3$@graphene/CNT electrode. In addition, no obvious voltage drop is noted, illustrating the low internal resistance of the $MnCO_3$@graphene/CNT electrode. Figure 4d compares the specific capacitance values of the $MnCO_3$@graphene (Figure S5) and $MnCO_3$@graphene/CNT electrodes as a function of current density. The capacitances for $MnCO_3$@graphene/CNT and $MnCO_3$@graphene electrode at current densities of 1, 3, 5, and 10 A g^{-1} are 467.2, 438, 414, and 394 F g^{-1} and 322.1, 282, 254, and 215.8 F g^{-1}, respectively. Meanwhile, the $MnCO_3$@graphene/CNT electrode has approximately 84.3% retention when the current density increases from 1 to 10 A g^{-1}, which is higher than the approximate retention of the $MnCO_3$@graphene electrode, which is 67%. To further investigate ion/charge transfer kinetics of the samples, EIS was performed, as presented in Figure 4e. The results indicate that the $MnCO_3$@graphene/CNT show lower equivalent series resistance (1.3 **Ω**) than the $MnCO_3$@graphene (1.7 **Ω**), as obtained from the intercept of the Nyquist plots. In the Nyquist plots, smaller semicircle diameter and steeper liner slope for $MnCO_3$@graphene/CNT indicate lower charge transfer resistance and faster ion transfer for the $MnCO_3$@graphene/CNT electrode, respectively. The $MnCO_3$@graphene/CNT electrode exhibits that 88.1% of the initial capacitance of the $MnCO_3$@graphene/CNT electrode was retained after 6000 charge–discharge cycles at 5 A g^{-1},

revealing that the electrode has a very good long-term stability, which is important for practical applications (Figure 4f). This retention is higher than that of $MnCO_3$@graphene electrode (77.3%). Remarkably, the superior electrochemical performances of the $MnCO_3$@graphene/CNT electrodes are highly comparable with those of other $MnCO_3$–based electrodes reported previously (Table S1).

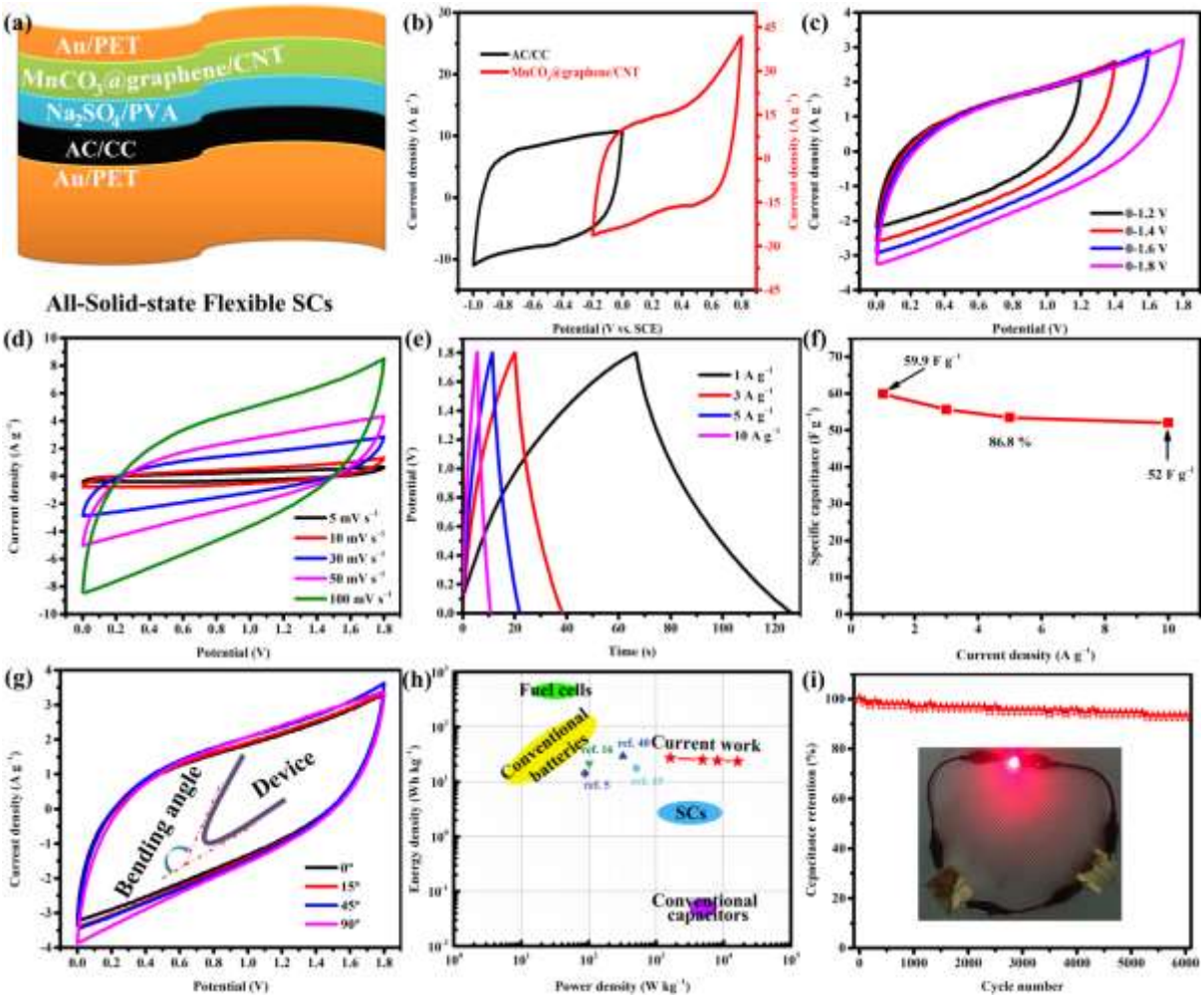

Figure 5. (a) Schematic of the assembled structure of a flexible all-solid-state asymmetric supercapacitor. (b) CV curves of the $MnCO_3$@graphene/CNT electrode and the AC/CC electrode at a scan rate of 50 mV s^{-1}. (c) CV curves of the $MnCO_3$@graphene/CNT//AC/CC asymmetric supercapacitors in different upper potentials from 1.2 V to 1.8 V at a scan rate of 50 mV s^{-1}. (d) CV curves of the flexible devices at different scan rates. (e) GCD curves of the flexible devices at various current densities. (f) Specific capacitance at different current

densities. (g) CV curves at different bending angles. (h) Ragone plots of the $MnCO_3$@graphene/CNT//CC/AC flexible device and previously reported $MnCO_3$-based supercapacitors. (i) Cycling performance of the device over 6000 cycles at 5 A g^{-1}. Inset: Red LED powered by two devices in the series.

To further evaluate the $MnCO_3$@graphene/CNT electrode for practical application, a flexible ASC device was assembled using the $MnCO_3$@graphene/CNT as the positive electrode, the AC on CC as the negative electrode (the details can be found in the Experimental Section and Figure S6), and the Na_2SO_4/PVA as separator and electrolyte (Figure 5a). Given that the $MnCO_3$@graphene/CNT electrode and the CC/AC electrode possess stable potential window of −1.0 V to 0.0 V and −0.2 V to 0.8 V, respectively (Figure 5b), the operating voltage of the flexible ASC can be extended to 1.8 V (Figure 5c). The CV curves of the flexible ASC devices were measured at various scan rates under 1.8 V (Figure 5d). All the CV curves exhibit approximately semi-rectangular shapes without any obvious redox peaks, indicating good reversibility and typical capacitive characteristics of our device. GCD curves collected at different current densities are near triangle-shaped curves (Figure 5e), signifying capacitive characteristic. The device exhibited high capacitance of 59.9 F g^{-1} at a current density of 1 A g^{-1} (Figure 5f). By increasing the current density to 10 A g^{-1}, a capacitance of 52 F g^{-1} is retained, which corresponds to a capacitance retention of 86.8% of its initial value. Figure 5g shows that the CV curves remain almost the same at a scan rate of 50 mV s^{-1} under different bending angles of 15°, 45°, and 90°, suggesting that the integrity of the flexible ASC during bending. A slight increase in capacitance can be attributed to the reduced distance between two electrodes, which helps improve conductivity and ion transport during bending.[39] The energy and power densities of $MnCO_3$@graphene/CNT//CC/AC flexible device were further evaluated for practical application. As displayed in the Ragone plot (Figure 5h), the device

shows high energy density of 27 Wh kg^{-1} at a power density of 1622.7 W kg^{-1}. Even at a high-power density of 16200 W kg^{-1}, the device still delivers an energy density of 23.4 Wh kg^{-1}. These values are comparable to the previously reported $MnCO_3$-based supercapacitors, such as $MnO_2/MnCO_3$//rGO (17.8 Wh kg^{-1} at 400 W kg^{-1})[15], $MnCO_3$@MnO_2//rGO (27.4 Wh kg^{-1} at 271.7 W kg^{-1})[40], rGO-CNF-$MnCO_3$//rGO (21 Wh kg^{-1} at 102 W kg^{-1})[16], $MnCO_3$//porous carbon (14.7 Wh kg^{-1} at 90.2 W kg^{-1})[5]. The cycling test shows that the device maintains high capacity retention of 93% at a current density of 5 A g^{-1} for 6000 cycles, indicating excellent electrochemical stability (Figure 5i). Moreover, two ASC devices connected in the series can light up a red LED (inset of Figure 5i).

CONCLUSIONS

In summary, unique $MnCO_3$@graphene composites, in which the $MnCO_3$ nanorod is well confined in the graphene, have been successfully fabricated for the first time. Flexible and self-standing $MnCO_3$@graphene/CNT film is prepared through vacuum filtration to avoid the use of cumbersome current collector. The flexible $MnCO_3$@graphene/CNT film exhibits a high electrochemical performance (467.2 F g^{-1} at 1 A g^{-1}). Moreover, a flexible asymmetric all-solid-state $MnCO_3$@graphene/CNT//CC/AC supercapacitor, which delivers a high energy density of 27 Wh kg^{-1} and excellent stability (93% capacitance retention over 6000 cycles, is further constructed. This work offers a new insight to general material designs toward the efficient fabrication of electrodes for flexible electrochemical energy storage.

REFERENCES

(1) Wu, S. X.; Hui, K. S.; Hui, K. N., 2D Black Phosphorus: from Preparation to Applications for Electrochemical Energy Storage. *Adv. Sci* . **2018**, *5* (5), 1700491.

(2) Guo, R. S.; Chen, J. T.; Yang, B. J.; Liu, L. Y.; Su, L. J.; Shen, B. S.; Yan, X. B., In-Plane Micro-Supercapacitors for an Integrated Device on One Piece of Paper. *Adv. Funct. Mater.* **2017**, *27* (43), 1702394.

(3) Kim, S. W.; Kang, K. N.; Min, J. W.; Jang, J. H., Plotter-Assisted Integration of Wearable All-Solid-State Micro-Supercapacitors. *Nano Energy* **2018**, *50*, 410-416.

(4) Liu, C. Y.; Zhao, S. L.; Lu, Y. N.; Chang, Y. X.; Xu, D. D.; Wang, Q.; Dai, Z. H.; Bao, J. C.; Han, M., 3D Porous Nanoarchitectures Derived from SnS/S-Doped Graphene Hybrid Nanosheets for Flexible All-Solid-State Supercapacitors. *Small* **2017**, *13* (12) 1603494.

(5) Tang, Y. F.; Chen, S. J.; Chen, T.; Guo, W. F.; Li, Y. S.; Mu, S. C.; Yu, S. X.; Zhao, Y. F.; Wen, F. S.; Gao, F. M., Synthesis of Peanut-Like Hierarchical Manganese Carbonate Microcrystals via Magnetically Driven Self-Assembly for High Performance Asymmetric Supercapacitors. *J. Mater. Chem. A* **2017**, *5* (8), 3923-3931.

(6) Devaraj, S.; Liu, H. Y.; Balaya, P., $MnCO_3$: A Novel Electrode Material for Supercapacitors. *J .Mater. Chem. A* **2014**, *2* (12), 4276-4281.

(7)Zhang, N.; Ma, J. M.; Li, Q.; Li, J.; Ng, D. H. L., Shape-Controlled Synthesis of $MnCO_3$ Nanostructures and Their Applications in Supercapacitors. *RSC. Adv.* **2015**, *5* (100), 81981-81985.

(8) Zhou, L. K.; Kong, X. H.; Gao, M.; Lian, F.; Li, B. J.; Zhou, Z. F.; Cao, H. Q., Hydrothermal Fabrication of $MnCO_3$@rGO Composite as an Anode Material for High-Performance Lithium Ion Batteries. *Inorg. Chem.* **2014**, *53* (17), 9228-9234.

(9) Cui, G. L.; Hu, Y. S.; Zhi, L. J.; Wu, D. Q.; Lieberwirth, I.; Maier, J.; Mullen, K., A One-Step Approach Towards Carbon-Encapsulated Hollow Tin Nanoparticles and Their Application in Lithium Batteries. *Small* **2007**, *3* (12), 2066-2069.

(10) Wu, S. X.; Hui, K. S.; Hui, K. N.; Kim, K. H., Electrostatic-Induced Assembly of Graphene-Encapsulated Carbon@Nickel-Aluminum Layered Double Hydroxide Core-Shell Spheres Hybrid Structure for High-Energy and High-Power-Density Asymmetric Supercapacitor. *ACS Appl. Mater. Interfaces* **2017,** *9* (2), 1395-1406.

(11) Novoselov, K. S.; Geim, A. K.; Morozov, S. V.; Jiang, D.; Katsnelson, M. I.; Grigorieva, I. V.; Dubonos, S. V.; Firsov, A. A., Two-Dimensional Gas of Massless Dirac Fermions in Graphene. *Nature* **2005**, *438* (7065), 197-200.

(12) Fasolino, A.; Los, J. H.; Katsnelson, M. I., Intrinsic Ripples in Graphene. *Nat. Mater.* **2007**, *6* (11), 858-861.

(13) Yang, S. B.; Feng, X. L.; Wang, L.; Tang, K.; Maier, J.; Mullen, K., Graphene-Based Nanosheets with a Sandwich Structure. *Angew. Chem. Int. Edit.* **2010**, *49* (28), 4795-4799.

(14) Ghosh, D.; Giri, S.; Dhibar, S.; Das, C. K., Reduced Graphene Oxide/Manganese Carbonate Hybrid Composite: High Performance Supercapacitor Electrode Material. *Electrochim. Acta* **2014**, *147*, 557-564.

(15) Liu, Y. C.; He, D. W.; Wu, H. L.; Duan, J. H.; Zhang, Y. N., Hydrothermal Self-assembly of Manganese Dioxide/Manganese Carbonate/Reduced Graphene Oxide Aerogel for Asymmetric Supercapacitors. *Electrochim. Acta* **2015**, *164*, 154-162.

(16) Amutha, B.; Sathish, M., A 2 V Asymmetric Supercapacitor Based on Reduced Graphene Oxide-Carbon Nanofiber-Manganese Carbonate Nanocomposite and Reduced Graphene Oxide in Aqueous Solution. *J. Solid State Electr.* **2015**, *19* (8), 2311-2320.

(17) Yuan, J. J.; Zhu, J. W.; Bi, H. P.; Zhang, Z. Z.; Chen, S.; Liang, S. M.; Wang, X., Self-Assembled Hydrothermal Synthesis for Producing a $MnCO_3$/Graphene Hydrogel Composite and Its Electrochemical Properties. *RSC Adv.* **2013**, *3* (13), 4400-4407.

(18) Jana, M.; Kumar, J. S.; Khanra, P.; Samanta, P.; Koo, H.; Murmu, N. C.; Kuila, T., Superior Performance of Asymmetric Supercapacitor Based on Reduced Graphene Oxide-Manganese

Carbonate as Positive and Sono-Chemically Reduced Graphene Oxide as Negative Electrode Materials. *J. Power Sources* **2016**, *303*, 222-233.

(19) Hummers Jr, W. S.; Offeman, R. E., Preparation of Graphitic Oxide. *J. Am. Chem. Soc.* **1958**, *80* (6), 1339-1339.

(20) Kovtyukhova, N. I.; Ollivier, P. J.; Martin, B. R.; Mallouk, T. E.; Chizhik, S. A.; Buzaneva, E. V.; Gorchinskiy, A. D., Layer-by-Layer Assembly of Ultrathin Composite Films from Micron-Sized Graphite Oxide Sheets and Polycations. *Chem. Mater.* **1999**, *11* (3), 771-778.

(21) Wu, S. X.; Hui, K. S.; Hui, K. N., One-Dimensional Core-Shell Architecture Composed of Silver Nanowire@Hierarchical Nickel-Aluminum Layered Double Hydroxide Nanosheet as Advanced Electrode Materials for Pseudocapacitor. *J. Phys. Chem. C* **2015**, *119* (41), 23358-23365.

(22) Wu, S. X.; Hui, K. S.; Hui, K. N.; Kim, K. H., Ultrathin Porous NiO Nanoflake Arrays on Nickel Foam as An Advanced Electrode for High Performance Asymmetric Supercapacitors. *J. Mater. Chem. A* **2016**, *4* (23), 9113-9123.

(23) Pan, Z.; Liu, M.; Yang, J.; Qiu, Y.; Li, W.; Xu, Y.; Zhang, X.; Zhang, Y., High Electroactive Material Loading on a Carbon Nanotube@ 3D Graphene Aerogel for High-Performance Flexible All-Solid-State Asymmetric Supercapacitors. *Adv. Funct. Mater.* **2017**, 27, 1701122.

(24) Wang, X.; Li, Y. D., Synthesis and Formation Mechanism of Manganese Dioxide Nanowires/Nanorods. *Chem. Eur. J.* **2003**, *9* (1), 300-306.

(25) Alhabeb, M.; Beidaghi, M.; Van Aken, K. L.; Dyatkin, B.; Gogotsi, Y., High-Density Freestanding Graphene/Carbide-Derived Carbon Film Electrodes for Electrochemical Capacitors. *Carbon* **2017**, *118*, 642-649.

(26) Kang, W.; Yu, D. Y. W.; Li, W.; Zhang, Z.; Yang, X.; Ng, T. W.; Zou, R.; Tang, Y.; Zhang, W.; Lee, C. S., Nanostructured Porous Manganese Carbonate Spheres with Capacitive Effects

on the High Lithium Storage Capability. *Nanoscale* **2015**, *7* (22), 10146-10151.

(27) Kudin, K. N.; Ozbas, B.; Schniepp, H. C.; Prud'homme, R. K.; Aksay, I. A.; Car, R., Raman Spectra of Graphite Oxide and Functionalized Graphene Sheets. *Nano Lett.* **2008**, *8* (1), 36-41.

(28) Wang, B.; Al Abdulla, W.; Wang, D. L.; Zhao, X. S., A Three-Dimensional Porous $LiFePO_4$ Cathode Material Modified with a Nitrogen-Doped Graphene Aerogel for High-Power Lithium Ion Batteries. *Energ Environ. Sci.* **2015**, *8* (3), 869-875.

(29) Su, L. J.; Lei, S. L.; Liu, L.; Liu, L. Y.; Zhang, Y. F.; Shi, S. Q.; Yan, X. B., Sprinkling $MnFe_2O_4$ Quantum Dots on Nitrogen-Doped Graphene Sheets: the Formation Mechanism and Application for High-Performance Supercapacitor Electrodes. *J. Mater. Chem. A* **2018**, *6* (21), 9997-10007.

(30) Wu, F.; Li, J.; Su, Y. F.; Wang, J.; Yang, W.; Li, N.; Chen, L.; Chen, S.; Chen, R. J.; Bao, L. Y., Layer-by-Layer Assembled Architecture of Polyelectrolyte Multilayers and Graphene Sheets on Hollow Carbon Spheres/Sulfur Composite for High-Performance Lithium-Sulfur Batteries. *Nano Lett* **2016**, *16* (9), 5488-5494.

(31) Zhu, J. Y.; He, J. H., Facile Synthesis of Graphene-Wrapped Honeycomb MnO_2 Nanospheres and Their Application in Supercapacitors. *ACS Appl. Mater. Interfaces* **2012**, *4* (3), 1770-1776.

(32) Peng, S. J.; Li, L. L.; Han, X. P.; Sun, W. P.; Srinivasan, M.; Mhaisalkar, S. G.; Cheng, F. Y.; Yan, Q. Y.; Chen, J.; Ramakrishna, S., Cobalt Sulfide Nanosheet/Graphene/Carbon Nanotube Nanocomposites as Flexible Electrodes for Hydrogen Evolution. *Angew. Chem. Int. Edit.* **2014**, *53* (46), 12594-12599.

(33) Xiao, X.; Peng, X.; Jin, H. Y.; Li, T. Q.;Zhang, C. C.; Gao, B.; Hu, B.; Huo, K. F.; Zhou, J., Freestanding Mesoporous VN/CNT Hybrid Electrodes for Flexible All-Solid-State Supercapacitors. *Adv. Mater.* **2013**, *25* (36), 5091-5097.

(34) Wu, S. X.; San Hui, K.; Hui, K. N., Carbon Nanotube@Manganese Oxide Nanosheet Core-Shell Structure Encapsulated Within Reduced Graphene Oxide Film for Flexible All-Solid-State Asymmetric Supercapacitors. *Carbon* **2018**, *132*, 776-784.

(35) Wu, S. X.; Hui, K. S.; Hui, K. N.; Yun, J. M.; Kim, K. H., A Novel Approach to Fabricate Carbon Sphere Intercalated Holey Graphene Electrode for High Energy Density Electrochemical Capacitors. *Chem. Eng. J.* **2017**, *317*, 461-470.

(36) Zhao, L.; Yu, J.; Li, W. J.; Wang, S. G.; Dai, C. L.; Wu, J. W.; Bai, X. D.; Zhi, C. Y., Honeycomb Porous MnO_2 Nanofibers Assembled from Radially Grown Nanosheets for Aqueous Supercapacitors with High Working Voltage and Energy Density. *Nano Energy* **2014**, *4*, 39-48.

(37) Ko, W. Y.; Liu, Y. C.; Lai, J. Y.; Chung, C. C.; Lin, K. J., Vertically Standing MnO_2 Nanowalls Grown on AgCNT-Modified Carbon Fibers for High-Performance Supercapacitors. *ACS Sustainable Chem. Eng.* **2019**, *7* (1), 669-678.

(38) He, Q. Q.; Wang, H. Y.; Lun, N.; Qi, Y. X.; Liu, J. R.; Feng, J. K.; Qiu, J.; Bai, Y. J., Fabricating a Mn_3O_4/$Ni(OH)_2$ Nanocomposite by Water-Boiling Treatment for Use in Asymmetric Supercapacitors as an Electrode Material. *ACS Sustainable Chem. Eng.* **2018**, *6* (11), 15688-15696.

(39) Liu, Z. H.; Tian, X. C.; Xu, X.; He, L.; Yan, M. Y.; Han, C. H.; Li, Y.; Yang, W.; Mai, L. Q., Capacitance and Voltage Matching Between MnO_2 Nanoflake Cathode and Fe_2O_3 Nanoparticle Anode for High-Performance Asymmetric Micro-Supercapacitors. *Nano Res.* **2017**, *10* (7), 2471-2481.

(40) Chen, H.; Yan, Z.; Liu, X. Y.; Guo, X. L.; Zhang, Y. X.; Liu, Z. H., Rational Design of Microsphere and Microcube $MnCO_3$@MnO_2 Heterostructures for Supercapacitor Electrodes. *J. Power Sources* **2017**, *353*, 202-209.

FIGURE CAPTIONS

Figure 1. (a) Proposed $MnCO_3$@graphene evolution process. (b and c) SEM images and (d)

XRD pattern of $MnCO_3$@graphene, (e) crystal structure of $MnCO_3$. (f) Raman spectrum of $MnCO_3$@graphene. (g) XPS spectrum of Mn 2p.

Figure 2. (a, b, and c) TEM images of $MnCO_3$@graphene at different magnifications. The inset of (c) shows an HRTEM image of the $MnCO_3$@graphene. (d and e) HAADF-STEM image and corresponding elemental mapping images of $MnCO_3$@graphene. (f) EDX result of $MnCO_3$@graphene. Cu signals are from copper grid.

Figure 3. Schematics of the fabrication process of $MnCO_3$@graphene/CNT films: (a) CNT and stable CNT dispersion. (b) $MnCO_3$@graphene and stable $MnCO_3$@graphene dispersion. (c) CNT and $MnCO_3$@graphene hybrid and the stable hybrid dispersion. (d) Vacuum filtration was used in the fabrication process. (e) Digital photographs of the flexible and self-standing $MnCO_3$@graphene/CNT films and wrapping of glass rod. (f) Cross-section SEM image of the $MnCO_3$@graphene/CNT films with a thickness of 10 μm. (g) Supercapacitor applications of the $MnCO_3$@graphene/CNT films and schematic of the mechanism involved in the rapid electron transport and ion diffusion of the unique structure.

Figure 4. (a) Comparison of CV curves of two different electrodes at 50 mV s^{-1}. (b) CV curves of $MnCO_3$@graphene/CNT electrode at different scan rates. (c) GCD curves of $MnCO_3$@graphene/CNT electrode at different current densities. (d) Specific capacitances of the two electrodes at different current densities. (e) Nyquist plots of the electrodes. (f) Cycle performance of the two electrodes at 5 A g^{-1} for 6000 cycles.

Figure 5. (a) Schematic of the assembled structure of a flexible all-solid-state asymmetric supercapacitor. (b) CV curves of the $MnCO_3$@graphene/CNT electrode and the AC/CC electrode at a scan rate of 50 mV s^{-1}. (c) CV curves of the $MnCO_3$@graphene/CNT//AC/CC asymmetric supercapacitors in different upper potentials from 1.2 V to 1.8 V at a scan rate of 50 mV s^{-1}. (d) CV curves of the flexible devices at different scan rates. (e) GCD curves of the

flexible devices at various current densities. (f) Specific capacitance at different current densities. (g) CV curves at different bending angles. (h) Ragone plots of the $MnCO_3$@graphene/CNT//CC/AC flexible device and previously reported $MnCO_3$-based supercapacitors. (i) Cycling performance of the device over 6000 cycles at 5 A g^{-1}. Inset: Red LED powered by two devices in the series.

TOC GRAPHIC

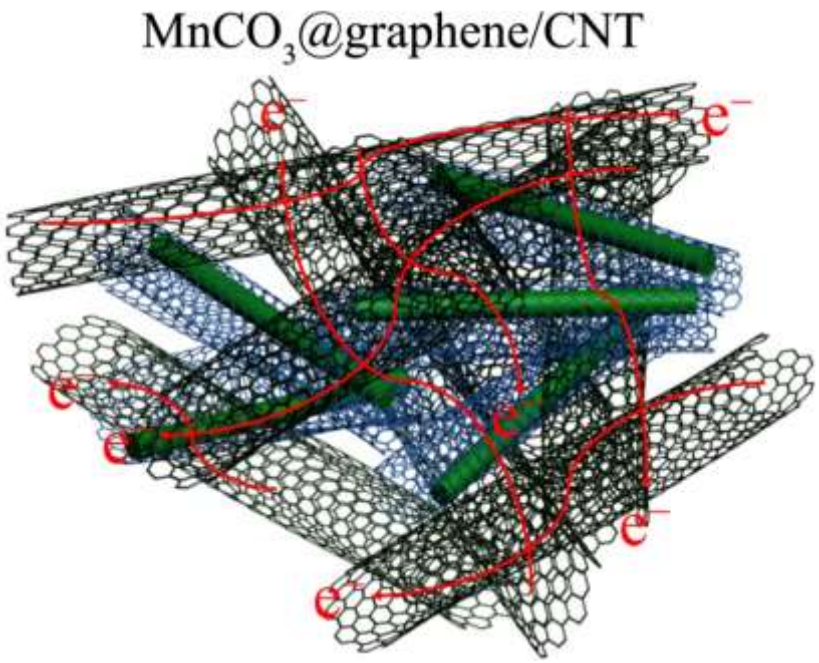

Synopsis

We report three-dimensional conductive network-based self-standing $MnCO_3$@graphene/CNT hybrid film as advanced electrode, which exhibits excellent electrochemical performance in flexible supercapacitors.